Mitral annulus segmentation from four-dimensional ultrasound using a valve state predictor and constrained optical flow

Robert J. Schneider[a,*], **Douglas P. Perrin**[a,b], **Nikolay V. Vasilyev**[b], **Gerald R. Marx**[c], **Pedro J. del Nido**[b], and **Robert D. Howe**[a]

[a]Harvard School of Engineering and Applied Sciences, Cambridge, MA, USA

[b]Department of Cardiac Surgery, Children's Hospital, Boston, MA, USA

[c]Department of Cardiology, Children's Hospital, Boston, MA, USA

Abstract

Measurement of the shape and motion of the mitral valve annulus has proven useful in a number of applications, including pathology diagnosis and mitral valve modeling. Current methods to delineate the annulus from four-dimensional (4D) ultrasound, however, either require extensive overhead or user-interaction, become inaccurate as they accumulate tracking error, or they do not account for annular shape or motion. This paper presents a new 4D annulus segmentation method to account for these deficiencies. The method builds on a previously published three-dimensional (3D) annulus segmentation algorithm that accurately and robustly segments the mitral annulus in a frame with a closed valve. In the 4D method, a valve state predictor determines when the valve is closed. Subsequently, the 3D annulus segmentation algorithm finds the annulus in those frames. For frames with an open valve, a constrained optical flow algorithm is used to the track the annulus. The only inputs to the algorithm are the selection of one frame with a closed valve and one user-specified point near the valve, neither of which needs to be precise. The accuracy of the tracking method is shown by comparing the tracking results to manual segmentations made by a group of experts, where an average RMS difference of 1.67 ± 0.63 mm was found across 30 tracked frames.

Keywords

Mitral valve; Annulus; Tracking; Segmentation; Ultrasound

1. Introduction

The mitral valve annulus is a fibrous saddle-shaped structure that anchors the mitral leaflets, and is critical to proper cardiac function. It is typically viewed in the clinical setting using four-dimensional (3D + time) ultrasound (4DUS), as ultrasound is inexpensive, portable, and non-ionizing. The shape and motion of the annulus are used in a number of applications, most commonly for pathology diagnosis, as it has been shown that the there is a strong correlation of annular shape and motion to several pathologies (Levine et al., 1989; Herregods et al., 1997; Flachskampf et al., 2000; Kaplan et al., 2000; Ahmad et al., 2004; Kaji et al., 2005; Popovic et al., 2005; Daimon et al., 2008; Alkadhi et al., 2009; Bothe et al.,

Appendix A. Supplementary data

Supplementary data associated with this article can be found, in the online version, at doi:10.1016/j.media.2011.11.006.

2008). It is also used as boundary conditions for mitral valve models (Kunzelman et al., 1993; Einstein et al., 2005; Lim et al., 2005; Votta et al., 2008; Hammer et al., 2008a,b), to assess valve function (Salgo et al., 2002; Jimenez et al., 2003), for surgical planning (Fabricius et al., 2004), and for implant design (Ferrazzi et al., 2009).

Methods to delineate annular shape and motion include tracking implanted radiopaque markers with fluoroscopy (Glasson et al., 1996; Dagum et al., 2001; Timek et al., 2003; Bothe et al., 2008), tracking implanted sonomicrometry transducers (Gorman et al., 1996), and time consuming manual segmentation from imaging (Levine et al., 1989; Herregods et al., 1997; Kaplan et al., 2000; Flachskampf et al., 2000; Ahmad et al., 2004; Kaji et al., 2005; Popovic et al., 2005; Daimon et al., 2008; Alkadhi et al., 2009; Qin et al., 2004; Saracino et al., 2004; Watanabe et al., 2006). Few automated methods have been developed to delineate its four-dimensional (4D) shape from ultrasound. There have been a number of semiautomatic methods to track the annulus in 2D ultrasound that generally require manual initialization of the mitral anatomy, after which the annulus points are tracked using some form of either block or template matching, optical flow, active contours, dynamic programming, or a combination of these methods (Eto et al., 2005; Takemoto et al., 2006; Martin et al., 2006; Nevo et al., 2007). One of the first methods to track the annulus in 4DUS is the work by Veronesi et al. (2006), which uses a combination of optical flow and block matching to track manually initialized annulus points in 4D. This method, however, does not constrain the motion of the annulus, leading the authors to add that "manual corrections were performed when required", revealing that the method accumulates tracking error that causes the delineations to become inaccurate. Ionasec et al. (2010) delineate the 4D annulus by fitting a mitral valve model to 4DUS data using machine learning techniques. The method, while accurate, requires an expansive database of thousands of manually delineated features (that took the authors two years to compile), making the method inaccessible to most.

Current 4D annulus delineation methods either require extensive user interaction, do not take into account the shape or motion of the annulus, or accumulate excessive tracking error. To address these issues, we present a new semi-automated 4D mitral annulus segmentation (4DMAS) method for delineating the annulus in a 4DUS sequence (Fig. 1). From the user, it requires only the selection of one frame with a closed valve and one point near the valve. Using these inputs and our previously-presented 3D mitral annulus segmentation (3DMAS) method for closed mitral valves (Schneider et al., 2010), the annulus in the selected frame is found. A valve state predictor then uses this annulus to determine those frames that contain a closed valve vs. those that contain an open valve. For those containing a closed valve, the 3DMAS method is again used. For those containing an open valve, a constrained optical flow formulation based on the Lucas and Kanade method (Lucas and Kanade, 1981) is used to track the annulus. In taking into account both the valve state and the shape and motion of the annulus in the optical flow method, the 4DMAS method limits the accumulation of segmentation error.

The details of the 4DMAS method are presented in Section 2. An analysis of the 4DMAS method is presented in Section 3, which includes studies that examine the accuracy of the valve state predictor (Section 3.1) and the accuracy of the constrained optical flow method (Section 3.2).

2. Materials and methods

2.1. 3D mitral annulus segmentation algorithm

The presented 4DMAS method builds on our previously developed 3DMAS algorithm, which is able to accurately segment the location of the annulus for closed mitral valves

(Schneider et al., 2010). It requires only the selection of a frame with a closed valve and a point near the center of the valve. The 3DMAS method ultimately provides the geometric prior of the annulus which we then track to frames with an open valve. The methods of computing a thin tissue detector and finding a leaflet surface, which were developed for the 3DMAS algorithm, are also used in the 4DMAS method to help determine the valve state throughout a sequence. The following sections explain how to integrate the 3DMAS method and its components into a 4D annulus tracking method that first predicts the valve state (open or closed) and then alters the segmentation approach based on valve state so that an accurate 4D annulus results with little accumulation of error due to tracking drift.

2.2. Valve state predictor

The 4DMAS method begins by first implementing the 3DMAS method on a user-specified frame using a specified point. The selected frame will be referred to as the reference frame, F_{ref}, and the resulting annulus as the reference annulus, A_{ref}. Predicting the valve state in all other frames is then done using information gathered from this segmentation. To begin, a mitral leaflet surface is computed in each frame as described in Schneider et al. (2010). Regardless of whether the valve is open or closed in a frame or whether the leaflets are visible or not, due to the nature of the surface generation method, which is a max-flow algorithm run on a cylindrically shaped graph surrounding the valve, a surface is always found in each frame (Fig. 2). When the valve is closed, the surface will reside at the leaflets, however, when the valve is open, the surface will reside somewhere in the blood pool formed by the left atrium and left ventricle. We then assume the value of the thin tissue detector and ultrasound intensity at the surface to be higher for closed valves than for open valves, and based on this we differentiate between the two states. Because we are not interested in the surface outside of the region of the valve, and because we know the valve moves roughly along an axis that we can estimate from A_{ref} (Kettler et al., 2007), we crop the surfaces in every frame by the projection of A_{ref} along the precomputed axis (Fig. 2), keeping only the region of the surfaces inside of the projected contour. We then compute the mean ultrasound intensity value, $\mu_{int,n}$, and mean thin tissue detector value, $\mu_{ttd,n}$, at the cropped surfaces. A valve score for each frame is then

$$VS_n = (\mu_{int,n})_{[0-1]} \, (\mu_{ttd,n})_{[0-1]} \tag{1}$$

where $(\cdot)_{[0-1]}$ indicates that the values for that term are normalized across all frames to the range of 0 to 1, and n indicates the frame number.

To group the frames into those that have a closed valve vs. those that have an open valve, the values of VS_n are clustered using a k-means clustering algorithm. Clusters are initialized by assigning all values greater than the mean of VS_n to the "closed valve" cluster, and all others to the "open valve" cluster. This is based on the assumption that closed valves will have a higher mean ultrasound intensity and thin tissue detector value at the cropped surface than open valves. The distance metric used for the k-means algorithm is the absolute value of the distance of each valve score to the mean of the respective clusters. Lastly, the valve score for F_{ref} is always assigned to the "closed valve" cluster to ensure a labeling consistent with the user's selection of a closed valve. An example of the clustering results for the ultrasound sequence shown in Fig. 2 can be seen in Fig. 3. For simplicity, frames containing a closed valve will herein be referred to as "closed frames", and similarly, frames containing an open valve as "open frames".

2.3. Annulus segmentation for closed valves

Knowing those images that contain closed valves via the valve state predictor, we segment the annulus in all closed frames using the 3DMAS algorithm. The initially provided point in

each frame that serves as the input to the algorithm is no longer provided by the user, but is determined automatically by projecting the center point of the originally segmented annulus along the valve axis onto the respective mitral leaflet surface that was used to compute the valve score.

2.4. Constrained optical flow

When the valve opens, it is no longer possible to segment the annulus using the 3DMAS method, and we must track the annulus from one frame to the other. Similar to previously published annulus tracking methods, we use a variation of the Lucas and Kanade optical flow (LKOF) algorithm, but unlike previous methods, we incorporate shape information in the formulation. A desirable characteristic of the LKOF method is the ability to compute the optical flow for individual points. This reduces the computational burden that other methods impose, such as the Horn and Schunck method (Horn and Schunck, 1981), which require the optical flow to be computed over an entire volume. We know the annulus is a continuous anatomical structure, and so we would like to enforce a locally smooth displacement of the annulus. However, unlike the Horn and Schunck method, the LKOF method is not equipped to enforce a locally smooth displacement field. We therefore modify the LKOF formulation to enforce this constraint for the purpose of tracking the mitral annulus.

The LKOF algorithm is based on the assumption that the intensity for a target location changes little from one frame to the next, and is formulated to minimize

$$E = \sum_{x \in R} [F(x+h) - G(x)]^2 \tag{2}$$

which is the sum of the squared differences for a small window, R, displaced by h in ultrasound intensity image F relative to image G. We want to track only the annulus from one frame to the next, and so refer to the displacement of point i along the annulus contour as $h_i = [h_{i1}, h_{i2}, h_{i3}]^T$. We know that h_i should exhibit small local deviations, and so in addition to minimizing the change in appearance of a window around a point, we also want to limit its movement based on the movement of neighboring points. We quantify the local deviations in annular displacement as $\partial^2 h_i / \partial s^2$, and therefore aim to minimize at each point

$$E_i = \sum_{x \in R} W(x) [F(x+h_i) - G(x)]^2 + \alpha \left(\frac{\partial^2 h_i}{\partial s^2}\right)^T \left(\frac{\partial^2 h_i}{\partial s^2}\right) \tag{3}$$

with respect to h_i, where α is a scalar weight. We refer to this method throughout the rest of this paper as the constrained Lucas and Kanade optical flow (CLKOF) method. For this formulation, the position along the annulus contour is parameterized by s. In the implementation, we track N evenly spaced points along the contour, making $i \in \{1, \ldots, N\}$. For this study, we use $N = 24$ and $\alpha = 500$. The weighting function

$$W(x) = \frac{\|\nabla \Omega(x)\|}{\sum_{x \in R} \|\nabla \Omega(x)\|} \tag{4}$$

is designed to give more importance to regions located at a high gradient magnitude, where Ω refers to the intensity of the ultrasound volume.

To find the h_i that minimizes (3), similar to approaches taken in Lucas and Kanade (1981) and Kass et al. (1988), we first approximate the first order derivative of F and second order derivative of h as

$$\frac{\partial}{\partial x}F(x) \approx \frac{F(x+h_i) - F(x)}{h_i} \tag{5}$$

$$\frac{\partial^2 h_i}{\partial s^2} \approx \frac{h_{i-1} - 2h_i + h_{i+1}}{\Delta s^2} \tag{6}$$

where $\frac{\partial}{\partial x} = \left[\frac{\partial}{\partial x_1}, \frac{\partial}{\partial x_2}, \frac{\partial}{\partial x_3}\right]$. We then substitute (5) and (6) into (3), making (7) the function to minimize. Setting $E_i/\ h_i = 0$ and solving for h_i, we get (8) as the solution for h_i, where I_3 is the 3×3 identity matrix.

$$E_i = \sum_{x \in R} W(x) \left[F(x) + h_i \frac{\partial}{\partial x}F(x) - G(x)\right]^2 + \alpha \left(\frac{h_{i-1} - 2h_i + h_{i+1}}{\Delta s^2}\right)^T \left(\frac{h_{i-1} - 2h_i + h_{i+1}}{\Delta s^2}\right) \tag{7}$$

$$h_i = \left[\sum_{x \in R}\left(\frac{\partial}{\partial x}F(x)\right)^T W(x)(G(x) - F(x)) + \frac{2\alpha}{\Delta s^4}(h_{i-1} + h_{i+1})\right] \times \left[\sum_{x \in R}\left(\frac{\partial}{\partial x}F(x)\right)^T W(x)\left(\frac{\partial}{\partial x}F(x)\right) + \frac{4\alpha}{\Delta s^4}I_3\right]^{-1} \tag{8}$$

$$h_i^{k+1} = \left[\sum_{x \in R}\left(\frac{\partial}{\partial x}F(x')\right)^T W(x)(G(x) - F(x')) + \frac{2\alpha}{\Delta s^4}\left(h_{i-1}^k + h_{i+1}^k\right)\right] \times \left[\sum_{x \in R}\left(\frac{\partial}{\partial x}F(x')\right)^T W(x)\left(\frac{\partial}{\partial x}F(x')\right) + \frac{4\alpha}{\Delta s^4}I_3\right]^{-1} \tag{8}$$

The solution to h_i is dependent on h_{i-1} and h_{i+1}, and so we solve for h_i by iterating (9), where $h_i^0 = 0$ and $x' = x + h_i^k$. However, as opposed to using a single window size to define R, we first use a large window to account for large displacements that may occur from frame to frame. We then use progressively smaller window sizes to stabilize and converge to a more accurate solution for h_i. For this study, we execute 50 iterations at window sizes of 11^3, 9^3, 7^3, 5^3, and 3^3, in that order. The tracked annulus, which is tracked from frame to frame starting from a closed frame, is then interpolated (spline interpolation) to create a continuous contour in space.

3. Results

The 4DMAS method consists of three major components: a valve state predictor, an annulus segmentation algorithm (3DMAS method), and an annulus tracking algorithm (CLKOF method). As we presented validation of the 3DMAS algorithm in Schneider et al. (2010), we present here an analysis of the valve state predictor and annulus tracking method. In the analysis, we used seven anonymized clinical transesophageal echocardiography sequences (iE33 Echocardiography System with X7–2t transesophageal probe, Philips Healthcare, Andover, MA, USA). To capture the entire mitral valve throughout the ultrasound sequence, these had to be acquired as EKG-gated full volume reconstructions. Volume dimensions were roughly $200 \times 200 \times 200$ voxels with a resolution of 0.5–0.75 mm/voxel. More details about the images and valves can be seen in Table 1.

An example of the results of the 4DMAS method are shown in Fig. 4 for the example sequence shown in Fig. 2. As a comparison, also shown in the figure are the results when tracking is performed with the original LKOF method vs. the CLKOF method, both using the window sizes and iterations as described. This highlights the stability of the CLKOF method vs. the LKOF method for annulus tracking in ultrasound.

The algorithm was coded mostly in MATLAB (The Math-Works, Natick, MA, USA), but used C++ for both computing parts of the thin tissue detector and for the implementation of the max-flow algorithm. In the validation studies, the parameter values used in the 3DMAS algorithm are the same as those listed in Schneider et al. (2010). The approximate time to compute the annulus for closed and open valves (64-bit PC, 3.0 GHz Intel Core 2 Duo processor with 4 GB of RAM) was roughly 90 and 30 s, respectively, which includes the time to determine valve states.

3.1. Valve state predictor accuracy study

Essential steps in computing the valve state predictor are finding the mitral leaflet surface in every frame, and then cropping the surfaces by the projection of A_{ref} segmented from the user-specified reference frame, F_{ref}. The valve state predictor is then dependent on F_{ref}. The user-specified point has no effect on the predictor, as the annulus segmentation in a closed frame is operator-independent for any reasonably placed point (Schneider et al., 2010). We therefore present here an analysis of the valve state predictor's accuracy and how it is affected by the user's choice of the reference frame.

For this study, we manually selected those frames that contained a closed valve (closed frames) vs. those that contained an open valve (open frames), where a closed valve was defined to be a valve with leaflets completely coapted. We considered each closed frame as a potential candidate for F_{ref} and subsequently computed the valve state predictor as described in Section 2.2 using each of these frames as F_{ref}. Because computing the valve state predictor is dependent on automatically computing A_{ref} using the 3DMAS method, which can only be done for closed valves, we did not consider open frames as a potential candidate for F_{ref}. The collective accuracy of the valve state predictor across all potential reference frames is shown in Table 2. This table shows that the valve state predictor was on average 99.2% accurate in identifying closed frames and 100% accurate in identifying open frames, suggesting that the predictor is insensitive to the choice of F_{ref} when it contains a closed valve.

3.2. 3D annulus tracking validation

3.2.1. CLKOF method vs. human observers—To assess the accuracy of the tracking method, we compared the annulus tracking results to manual delineations made by a group of three experts. We provided the experts with slices from 4DUS of the mitral valve, where slices were taken at 10 degree increments about the mitral axis. Within each image the experts had access to temporal information available from the entire ultrasound sequence.

As the 4DMAS method operates by tracking to open frames the annulus segmented automatically from a closed frame, we similarly asked the experts to do the same. We did this by providing the experts with the location of the automatically segmented annulus in the closed frames immediately neighboring the open frames. We then asked the experts to track the location of the displayed annulus to the neighboring frames containing an open mitral valve by clicking on the tracked annulus point locations in each slice. From the seven data sets, 30 frames total were used for this study. The manual tracking of an annulus from one frame to a neighboring frame took roughly 5 min on average across all participants and all tracked frames. A typical comparison between a manually and automatically tracked annulus is shown in Fig. 5.

We computed accuracy measures for the CLKOF method by measuring the distance of the automatically tracked annulus to the mean of the points delineated by the experts. The results from the analysis for each data set can be seen in Table 3, where it is shown that

across the seven data sets (30 frames total), there was an average RMS difference of 1.67 ± 0.63 mm of the algorithm annulus to the mean of the experts.

The previous analysis treats the expert mean as a gold standard as a means of computing an error for the CLKOF method, however, it is also important to gauge the relative performance of the group of experts and the algorithm to determine if there is a discernible difference between the two groups. To perform this analysis, we repeated the analysis that was done for the CLKOF method for each expert. The difference being that in this study, a given expert's segmentation was compared to the mean computed using the segmentations from the other two experts and the CLKOF algorithm, thereby treating the algorithm as an equal participant. The results of this analysis can be seen in Table 4. While the overall performance of the CLKOF method (RMS = 1.67 ± 0.63 mm, $n = 30$) was slightly better than that of the group of experts (RMS = 1.99 ± 1.15 mm, $n = 90$) in that the CLKOF method had a lower mean RMS distance, the difference between the two groups is not statistically significant ($p = 0.062$), suggesting that the CLKOF method performed at least as well as the group of experts.

3.2.2. CLKOF tracking method vs. 3DMAS method for a closed valve annulus

—We showed in Section 3.1 that when the valve state predictor mislabels a valve, it fails by mislabeling a closed valve as an open valve (Table 2, Data set 4). In this case, the CLKOF method is employed instead of using the 3DMAS algorithm. As the 3DMAS algorithm was shown in Schneider et al. (2010) to be highly accurate, it is important to know how much an automatically segmented annulus and a tracked annulus differ for a closed valve. A typical comparison of the resulting annuli from the two methods is shown in Fig. 6.

In this study, for each data set we randomly chose a frame with a closed valve and tracked the annulus to neighboring frames with a closed valve using the CLKOF method. Additionally, we computed the automated annulus segmentations for the same neighboring frames using the 3DMAS method. We then compared the different annulus delineations by computing the RMS distance between the two annulus point sets. The results of the analysis are shown in Table 5, where the average RMS difference across all data sets was found to be 0.58 ± 0.31 mm, which is on the order of the volume resolution.

4. Discussion

4.1. Performance and validation

The 4DMAS method is unique in that it constructs a 4D annulus by first detecting whether a valve is open or closed in a given frame so that the segmentation approach can be appropriately altered. We showed that the valve state predictor is highly accurate, with over 99% correct assignment to the correct state in validation tests. When the valve state predictor did not coincide with the manual clustering, it did so by predicting that a closed valve was actually an open valve, and was the result of the valve being in a transition state. In this case, the CLKOF method would be used to track the annulus from a neighboring frame to the mislabeled frame instead of using the 3DMAS method to automatically segment the annulus. We showed in our analysis that the average RMS difference between a tracked (CLKOF) annulus to a segmented (3DMAS) annulus for closed valves was 0.58 ± 0.31 mm, indicating that the penalty associated with mislabeling a closed valve as an open valve is small. A more significant failure would be if the valve state predictor mislabeled an open valve as a closed valve. In this case, the 3DMAS algorithm would be employed for an open valve, and because the 3DMAS algorithm was not designed for open valves, the error associated with this mislabeling is substantial.

The accuracy of the 4DMAS method is not only a result of being able to predict the valve state, but having predicted the valve state, using accurate methods to find the annulus. We showed in Schneider et al. (2010) that the 3DMAS algorithm is accurate and robust when finding the annulus for closed mitral valves. In this manuscript, we showed that the CLKOF tracking method is as accurate at segmenting the annulus of open valves. In comparing the automated tracking results to manual delineations made by a group of experts across 30 frames, we found an average RMS difference of 1.67 ± 0.63 mm. This is on the same order of accuracy as the 3DMAS method, which had an RMS difference of 1.81 ± 0.78 mm when compared to manual annulus delineations made by a group of 10 experts on 10 different valves. Additionally, we showed that when comparing the overall performance of the CLKOF algorithm (RMS = 1.67 ± 0.63 mm, $n = 30$) to that of the group of three experts (RMS = 1.99 ± 1.15 mm, $n = 90$), while the algorithm tended toward better performance, there was no statistically significant difference between the two groups ($p = 0.062$).

The CLKOF tracking method performs well for annulus tracking in ultrasound because it can compensate for noise and inhomogeneities in the ultrasound volume by taking advantage of the correlation between the motion of neighboring points. Referring back to (8), which is the solution for the displacement, h_i, of point i along the annulus, it follows that the contribution of the imaging and the prior knowledge about annular geometry are controlled by the scalar weight α. In setting α to zero, the solution for h_i is the same as originally derived by Lucas and Kanade (1981). In this case, tracking results are dependent entirely on the imaging. An example of the resulting annulus can be seen in the bottom row of Fig. 4. Conversely, if α is made to be large or if the imaging provides little information (i.e. $\frac{\partial F}{\partial x} \approx 0$), then $h_i \approx \frac{1}{2}(h_{i-1} + h_{i+1})$ (i.e. the displacement is the average of the displacement of the neighboring points). Therefore, assuming α is neither too small nor too large, the annulus tracking would be dictated mostly by the imaging in areas of high definition in the ultrasound volume, and by the geometric prior in areas of low definition. The result is a more stable and accurate tracking of the annulus. The implementation of a constrained optical flow algorithm has also shown to be useful in other previous applications such as face tracking (Decarlo and Metaxas, 2000) and left ventricle motion detection in MR images (Loncaric and Macan, 2000).

When compared to previous automated methods for 4D annulus segmentation from ultrasound (Veronesi et al., 2006 and Ionasec et al., 2010), the presented method offers notable improvements in several areas, the first of which is the amount of overhead and degree of user-interaction. Previous methods either required manual initialization of an annulus, intermittent manual corrections of an automated algorithm, or a large database of manually selected feature locations. Conversely, the 4DMAS method requires only the selection of a frame with a closed valve and a point near the center of that valve. Secondly, because of the accuracy of the valve state predictor and the insensitivity of the 3DMAS method, the results of the 4DMAS method are likewise insensitive to the user's input, resulting in an operator-independent 4D annulus segmentation. Lastly, the extensive analysis performed both on the 3DMAS method in Schneider et al. (2010), on the valve state predictor, and on the CLKOF tracking method make the 4DMAS method the most well validated 4D annulus segmentation algorithm.

4.2. Algorithm design

As alluded to in Section 2.1, the 3DMAS method is designed for ultrasound images where the thin leaflet tissue is visible. Additionally, both the 3DMAS and CLKOF methods are designed for when the entire mitral annulus is contained in the conical ultrasound volume. As a result, the 4DMAS method is designed for ultrasound images acquired with an en face view of the mitral valve and that contain the complete mitral annulus in the conical data

volume throughout the cardiac cycle. This is why the 4DMAS validation studies used EKG-gated full volume reconstruction images of the mitral valve. However, if similar views could be obtained with the higher temporal resolution as seen in live 3D acquisitions, these would be preferred.

While the 4DMAS relies on imaging to predict valve state, one might argue that using an EKG signal might prove to be simpler and just as effective, as there should be a correspondence between the signal and the valve state. However, there are many reasons why an image-based valve state predictor is preferred over the EKG signal. One reason is that the EKG signal can be adversely affected by many variables in the operating-room environment. Additionally, depending on disease states, the electrophysiology of the heart may not correspond to the valve state. For instance, in the case of systolic anterior motion, the mitral valve may in fact be pulled open during systole. It is then more reliable to use the appearance of the heart in imaging to predict state rather than make predictions based on correlations to electrophysiology.

In the CLKOF method, it is worth noting that the scalar weight α was tuned to a constant of 500, as this was found to adequately balance both the contribution of the imaging and the geometric prior. However, α need not be set to a constant, but could be determined dynamically as a function of position of an annulus point along the contour, local curvature of the contour, or local imaging characteristics. Given the accuracy of the current method, however, the benefit of this dynamic assignment is likely small.

A current limitation of the 4DMAS method is that, due to separate executions of the 3DMAS method on closed frames, a correspondence between annular points of neighboring closed frames is not inherent. Therefore, while the annular geometry is tracked as a whole throughout the cardiac cycle, specific annular points are not. We could compensate for this, however, by using geometric constraints and similarity measures, such as ultrasound intensity or thin tissue detector patterns, to determine a correspondence between annuli after they have been segmented.

4.3. Future work

The mitral annulus is an important cardiac structure that is widely studied both clinically and for research purposes. The presented method, being that it is accurate and requires little user interaction, could serve to expedite a number of new studies. Knowing the valve state in a frame could also prove valuable in future work to determine the temporal location of a frame relative to the cardiac cycle without using an EKG signal. This could be useful information in related segmentation efforts, such as mitral leaflet or left ventricle segmentation. Also, because the presented method can determine valve state and switch between direct segmentation and tracking, it does not accumulate substantial tracking error, and could be used to analyze longer ultrasound sequences than those studied.

Future work will also include addressing the limitations on the images for which the 4DMAS method will successfully and accurately segment the mitral annulus – in particular, the limitation that the entire mitral annulus needs to be contained in the ultrasound volume throughout the cardiac cycle. Currently, to obtain such an ultrasound sequence, EKG-gated full volume reconstructions are acquired. However, this consequently lowers the frame rate. It would be beneficial to design methods to construct large field-of-view images with high temporal resolution.

5. Conclusion

The presented 4D mitral annulus segmentation method is an accurate and robust means of delineating the annulus throughout a 4DUS sequence. It finds the 4D annulus by first using a valve state predictor to determine those frames that contain a closed valve vs. those that contain an open valve. We found that the valve state predictor was on average 99.2% accurate in identifying closed valves and 100% accurate in identifying open valves. For closed valves, our previously presented 3D annulus segmentation method is used to find the annulus. For open valves, a constrained optical flow algorithm is used that takes into account annular shape and motion. In comparing the tracking results of the CLKOF algorithm to manually tracked points, we found an average RMS difference of 1.67 ± 0.63 mm. While the CLKOF algorithm tended to outperform the experts, the difference between the two groups was not statistically significant ($p = 0.062$), suggesting that the algorithm performed at least as well as the experts. The 4D annulus segmentation method requires from the user only the selection of one frame with a closed valve and one point near the valve in that frame. We showed that resulting 4D annulus is essentially independent of these inputs.

Supplementary Material

Refer to Web version on PubMed Central for supplementary material.

Acknowledgments

References

Levine R, Handschumacher M, Sanfilippo A, Hagege A, Harrigan P, Marshall J, Weyman A. Three-dimensional echocardiographic reconstruction of the mitral valve, with implications for the diagnosis of mitral valve prolapse. Circulation. 1989; 80(3):589–598. [PubMed: 2766511]

Herregods M, Tau A, Vandeplas A, Bijnens B, Van de Werf F. Values for mitral valve annulus dimensions in normals and patients with mitral regurgitation. Echocardiography. 1997; 14(6 Pt 1): 529–534. [PubMed: 11174991]

Flachskampf F, Chandra S, Gaddipatti A, Levine R, Weyman A, Ameling W, Hanrath P, Thomas J. Analysis of shape and motion of the mitral annulus in subjects with and without cardiomyopathy by echocardiographic 3-dimensional reconstruction. Journal of the American Society of Echocardiography. 2000; 13(4):277–287. [PubMed: 10756245]

Kaplan S, Bashein G, Sheehan F, Legget M, Munt B, Li X, Sivarajan M, Bolson E, Arch M, Martin R. Three-dimensional echocardiographic assessment of annular shape changes in the normal and regurgitant mitral valve. American Heart Journal. 2000; 139(3):378–387. [PubMed: 10689248]

Ahmad R, Gillinov A, McCarthy P, Blackstone E, Apperson-Hansen C, Qin J, Agler D, Shiota T, Cosgrove D. Annular geometry and motion in human ischemic mitral regurgitation: novel assessment with three-dimensional echocardiography and computer reconstruction. The Annals of Thoracic Surgery. 2004; 78(6):2063–2068. [PubMed: 15561036]

Kaji S, Nasu M, Yamamuro A, Tanabe K, Nagai K, Tani T, Tamita K, Shiratori K, Kinoshita M, Senda M, et al. Annular geometry in patients with chronic ischemic mitral regurgitation: three-dimensional magnetic resonance imaging study. Circulation. 2005; 112(9 Suppl.):I409–I414. [PubMed: 16159855]

Popovic Z, Martin M, Fukamachi K, Inoue M, Kwan J, Doi K, Qin J, Shiota T, Garcia M, McCarthy P, et al. Mitral annulus size links ventricular dilatation to functional mitral regurgitation. Journal of the American Society of Echocardiography. 2005; 18(9):959–963. [PubMed: 16153522]

Daimon M, Saracino G, Gillinov A, Koyama Y, Fukuda S, Kwan J, Song J, Kongsaerepong V, Agler D, Thomas J, et al. Local dysfunction and asymmetrical deformation of mitral annular geometry in ischemic mitral regurgitation: a novel computerized 3D echocardiographic analysis. Echocardiography. 2008; 25(4):414–423. [PubMed: 18177391]

Alkadhi H, Desbiolles L, Stolzmann P, Leschka S, Scheffel H, Plass A, Schertler T, Trindade P, Genoni M, Cattin P, et al. Mitral annular shape, size, and motion in normals and in patients with cardiomyopathy: evaluation with computed tomography. Investigative Radiology. 2009; 44(4):218–225. [PubMed: 19212270]

Bothe W, Nguyen T, Ennis D, Itoh A, Carlhäll C, Lai D, Ingels N, Miller D. Effects of acute ischemic mitral regurgitation on three-dimensional mitral leaflet edge geometry. European Journal of Cardio-Thoracic Surgery. 2008; 33(2):191–197. [PubMed: 18321461]

Kunzelman KS, Cochran RP, Chuong C, Ring WS, Verrier ED, Eberhart RD. Finite element analysis of the mitral valve. The Journal of Heart Valve Disease. 1993; 2(3):326–340. [PubMed: 8269128]

Einstein D, Kunzelman K, Reinhall P, Nicosia M, Cochran R. Non-linear fluid-coupled computational model of the mitral valve. The Journal of Heart Valve Disease. 2005; 14(3):376–385. [PubMed: 15974533]

Lim K, Yeo J, Duran C. Three-dimensional asymmetrical modeling of the mitral valve: a finite element study with dynamic boundaries. The Journal of Heart Valve Disease. 2005; 14(3):386–392. [PubMed: 15974534]

Votta E, Caiani E, Veronesi F, Soncini M, Montevecchi F, Redaelli A. Mitral valve finite-element modelling from ultrasound data: a pilot study for a new approach to understand mitral function and clinical scenarios. Philosophical Transactions of the Royal Society London, Series A. 2008; 366(1879):3411–3434.

Hammer, P.; Vasilyev, N.; Perrin, D.; del Nido, P.; Howe, R. Fast image-based model of mitral valve closure for surgical planning; MICCAI 2008 Workshop Proceedings: Computational Biomechanics for Medicine III; New York, NY. 2008a. p. 15-26.

Hammer P, Perrin D, Pedro J, Howe R. Image-based mass-spring model of mitral valve closure for surgical planning. Proc. SPIE – Medical Imaging. 2008b; vol. 6918:69180Q1–69180Q8.

Salgo I, Gorman J, Gorman R, Jackson B, Bowen F, Plappert T, St John Sutton M, Edmunds L. Effect of annular shape on leaflet curvature in reducing mitral leaflet stress. Circulation. 2002; 106(6):711–717. [PubMed: 12163432]

Jimenez J, Soerensen D, He Z, He S, Yoganathan A. Effects of a saddle shaped annulus on mitral valve function and chordal force distribution: an in vitro study. Annals of Biomedical Engineering. 2003; 31(10):1171–1181. [PubMed: 14649491]

Fabricius A, Walther T, Falk V, Mohr F. Three-dimensional echocardiography for planning of mitral valve surgery: current applicability? The Annals of Thoracic Surgery. 2004; 78(2):575–578. [PubMed: 15276524]

Ferrazzi P, Iacovoni A, Pentiricci S, Senni M, Iascone M, Borenstein N, Behr L, Borghi A, Balossino R, Quaini E. Toward the development of a fully elastic mitral ring: preliminary, acute, in vivo evaluation of physiomechanical behavior. The Journal of Thoracic and Cardiovascular Surgery. 2009; 137(1):174–179. [PubMed: 19154922]

Glasson J, Komeda M, Daughters G, Niczyporuk M, Bolger A, Ingels N, Miller D. Three-dimensional regional dynamics of the normal mitral anulus during left ventricular ejection. The Journal of Thoracic and Cardiovascular Surgery. 1996; 111(3):574–585. [PubMed: 8601972]

Dagum P, Timek T, Green G, Daughters G, Liang D, Ingels N, Miller D. Three-dimensional geometric comparison of partial and complete flexible mitral annuloplasty rings. The Journal of Thoracic and Cardiovascular Surgery. 2001; 122(4):665–673. [PubMed: 11581596]

Timek T, Dagum P, Lai D, Liang D, Daughters G, Tibayan F, Ingels N, Miller D. Tachycardia-induced cardiomyopathy in the ovine heart: mitral annular dynamic three-dimensional geometry. The Journal of Thoracic and Cardiovascular Surgery. 2003; 125(2):315–324. [PubMed: 12579100]

Gorman J, Gupta K, Streicher J, Gorman R, Jackson B, Ratcliffe M, Bogen D, Edmunds L. Dynamic three-dimensional imaging of the mitral valve and left ventricle by rapid sonomicrometry array localization. The Journal of Thoracic and Cardiovascular Surgery. 1996; 112(3):712–726. [PubMed: 8800160]

Qin J, Shiota T, Tsujino H, Saracino G, White R, Greenberg N, Kwan J, Popovic Z, Agler D, Stewart W, et al. Mitral annular motion as a surrogate for left ventricular ejection fraction: real-time three-dimensional echocardiography and magnetic resonance imaging studies. European Journal of Echocardiography. 2004; 5(6):407–415. [PubMed: 15556815]

Saracino G, Daimon M, Greenberg N, Shiota T, Thomas J. A novel system for the assessment of mitral annular geometry and analysis of 3D motion of mitral annulus from 3D echocardiography. Computers in Cardiology. 2004; 31:69–72.

Watanabe N, Ogasawara Y, Yamaura Y, Yamamoto K, Wada N, Okahashi N, Kawamoto T, Toyota E, Yoshida K. Dynamics of mitral complex geometry and functional mitral regurgitation during heart failure treatment. Journal of Echocardiography. 2006; 4(2):51–58.

Eto Y, Yamada H, Shin J, Agler D, Tsujino H, Qin J, Saracino G, Greenberg N, Thomas J, Shiota T. Automated mitral annular tracking: a novel method for evaluating mitral annular motion using two-dimensional echocardiography. Journal of the American Society of Echocardiography. 2005; 18(4):306–312. [PubMed: 15846156]

Takemoto Y, Hozumi T, Sugioka K, Watanabe H, Matsumura Y, Yoshiyama M, Takeuchi K, Yoshikawa J. Automated three-dimensional analysis of mitral annular dynamics in patients with myocardial infarction using automated mitral annular tracking method. Echocardiography. 2006; 23(8):658–665. [PubMed: 16970717]

Martin S, Daanen V, Chavanon O, Troccaz J. Fast Segmentation of the Mitral Valve Leaflet in Echocardiography. Lecture Notes in Computer Science – Computer Vision Approaches to Medical Image Analysis. 2006; vol. 4241:225–235.

Nevo S, van Stralen M, Vossepoel A, Reiber J, de Jong N, van der Steen A, Bosch J. Automated tracking of the mitral valve annulus motion in apical echocardiographic images using multidimensional dynamic programming. Ultrasound in Medicine & Biology. 2007; 33(9):1389–1399. [PubMed: 17513035]

Veronesi F, Corsi C, Caiani E, Sugeng L, Weinert L, Mor-Avi V, Lang R, Lamberti C. Semi-automatic tracking for mitral annulus dynamic analysis using real-time 3D echocardiography. Computers in Cardiology. 2006; 33:113–116.

Ionasec R, Voigt I, Georgescu B, Wang Y, Houle H, Vega-Higuera F, Navab N, Comaniciu D. Patient-specific modeling and quantification of the aortic and mitral valves from 4-D cardiac CT and TEE. IEEE Transactions on Medical Imaging. 2010; 29(9):1636–1651. [PubMed: 20442044]

Schneider R, Perrin D, Vasilyev N, Marx G, del Nido P, Howe R. Mitral annulus segmentation from 3D ultrasound using graph cuts. IEEE Transactions on Medical Imaging. 2010; 29(9):1676–1687. [PubMed: 20562042]

Lucas, B.; Kanade, T. An iterative image registration technique with an application to stereo vision; Proc. 7th International Joint Conference on Artificial Intelligence; Vancouver, BC, Canada. 1981. p. 674-679.

Kettler, D.; Plowes, R.; Novotny, P.; Vasilyev, N.; del Nido, P.; Howe, R. An active motion compensation instrument for beating heart mitral valve surgery; Proc. IEEE International Conference on Intelligent Robots and Systems; 2007. p. 1290-1295.

Horn B, Schunck B. Determining optical flow. Artificial Intelligence. 1981; 17:185–203.

Kass M, Witkin A, Terzopoulos D. Snakes: active contour models. International Journal of Computer Vision. 1988; 1(4):321–331.

Decarlo D, Metaxas D. Optical flow constraints on deformable models with applications to face tracking. International Journal of Computer Vision. 2000; 38(2):99–127.

Loncaric S, Macan T. Point-constrained optical flow for LV motion detection. Proceedings of SPIE. 2000; vol. 3978:521–529.
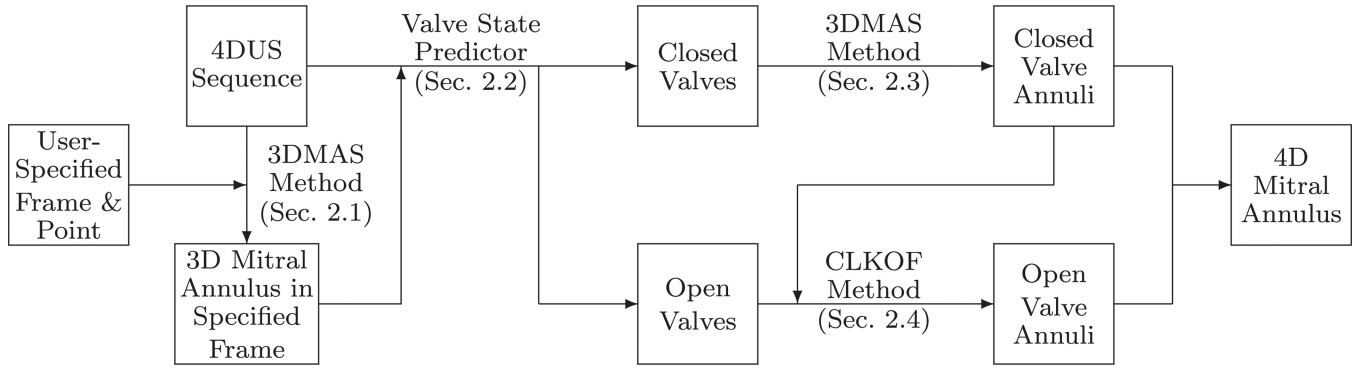
Fig. 1.
Flow chart outlining the new 4D mitral annulus segmentation (4DMAS) algorithm. Specific details for the respective processes can be found in the indicated sections.
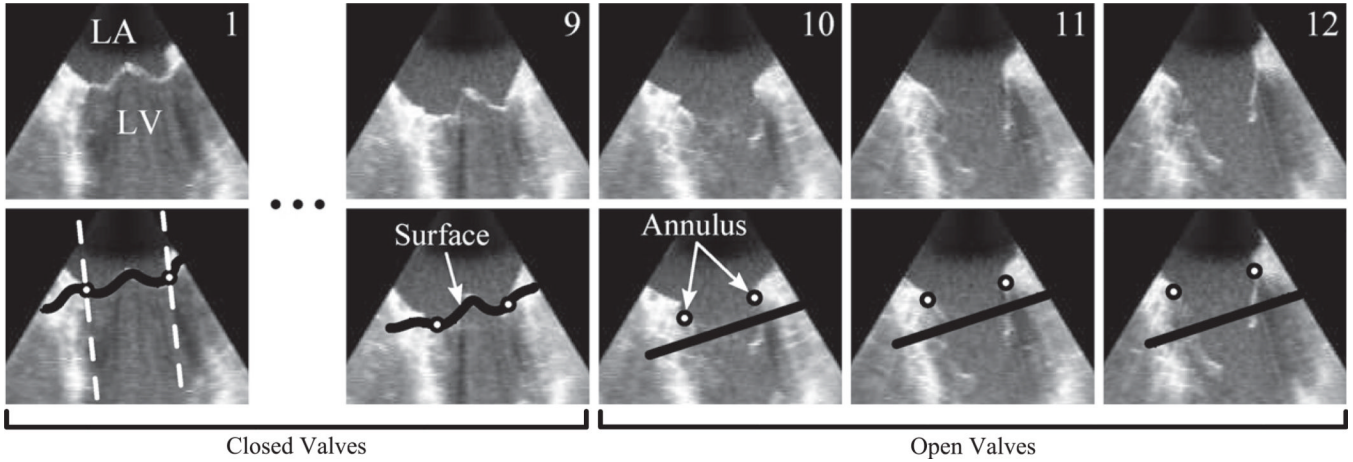
Fig. 2.
(*Top row*) Slices from a 4DUS sequence showing a prolapsed mitral valve over a cardiac cycle, where the numbers indicate the frame number. (*Bottom row*) The same slices from the top row shown with the surfaces used in the valve state prediction, and the final location of the segmented annulus. The white dashed lines in the bottom left image indicate the cropping boundaries used in the valve state prediction, and are formed by the projection of A_{ref} along the valve axis. This boundary is constant for all frames. The closed and open valves are those as determined by the valve state predictor. It can be seen that when the valve opens, the surface cannot find closed leaflets and so resides in the blood pool. The annulus is then found by tracking instead of direct segmentation (LA – left atrium; LV – left ventricle).
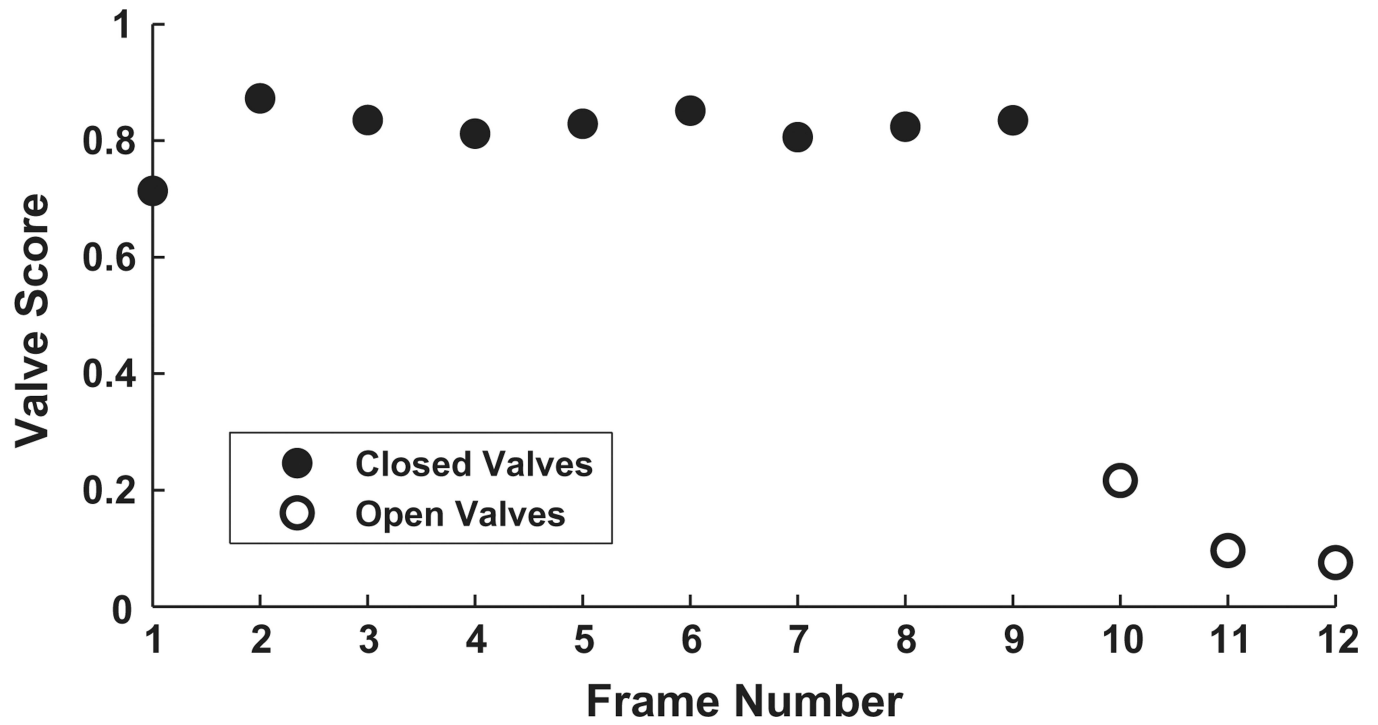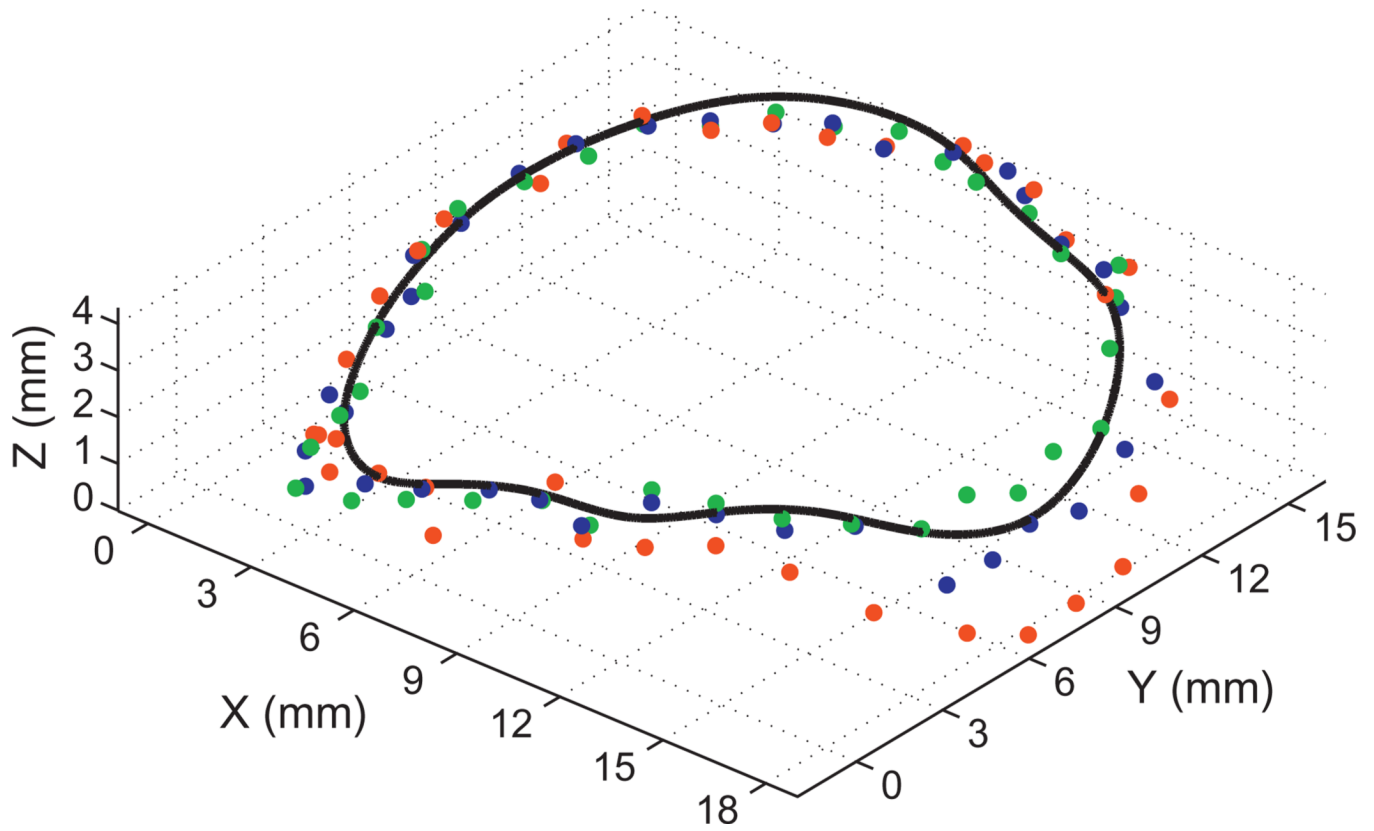
Fig. 3.
Mitral valve scores for the 4DUS sequence shown in Fig. 2 using Frame 1 as the reference frame.
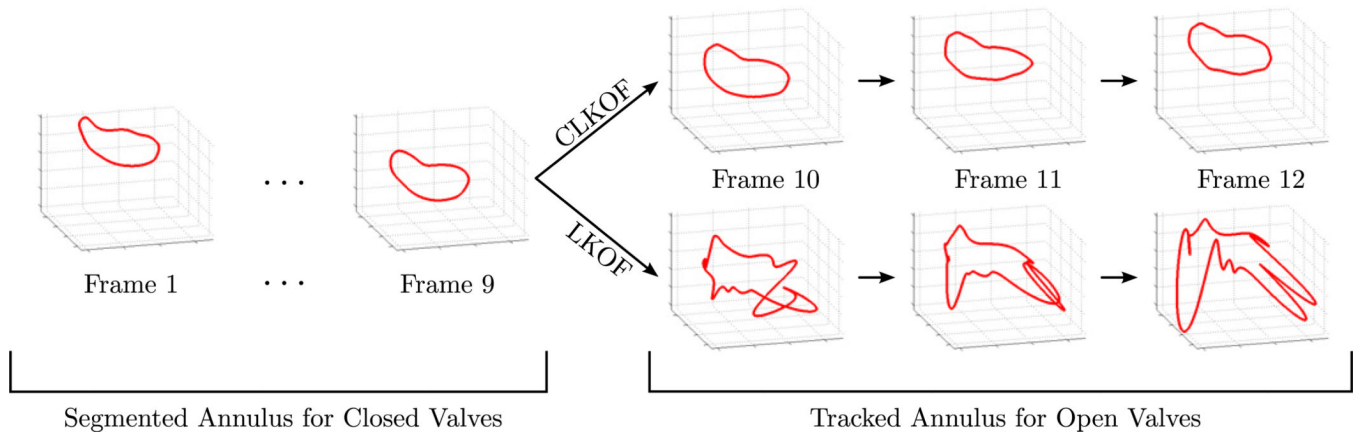
Fig. 4.
Comparison of the resulting 4D annulus delineation for the example 4DUS sequence shown in Fig. 2 when tracking is performed using the original LKOF method (i.e. minimizing (2)) vs. the CLKOF method (i.e. minimizing (3)).

Fig. 5.
Typical comparison between the annulus tracked by the human observers (colored points) and that tracked using the CLKOF method (solid contour). (For interpretation of the references to colour in this figure legend, the reader is referred to the web version of this article.)
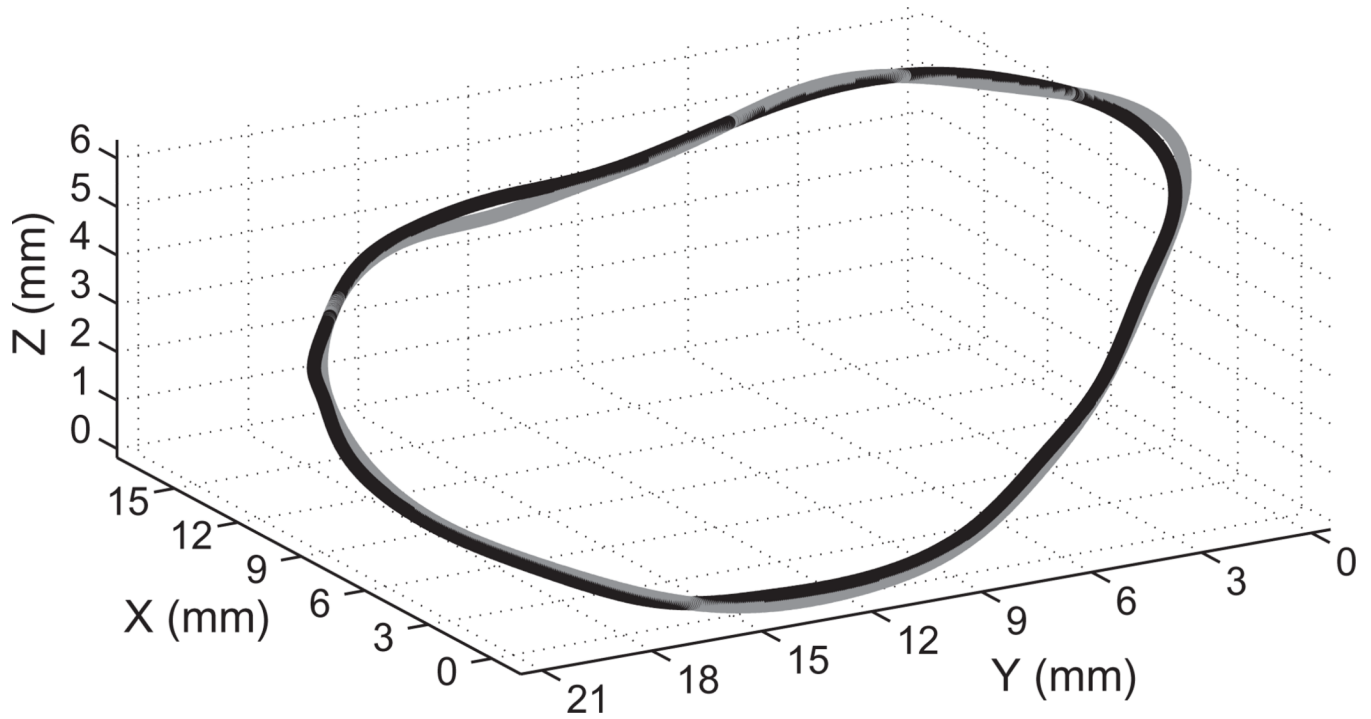
Fig. 6.
Typical comparison between an annulus delineated using the CLKOF tracking method
(black) and the 3DMAS method (gray) for a closed valve.

Table 1

Summary of clinical mitral valve images used in the validation studies.

Valve	Mitral valve state	Frames in sequence
1	Prolapse; regurgitation	12
2	Prolapse; dilated annulus	20
3	Normal	11
4	Normal	15
5	Cleft mitral	16
6	Normal	13
7	Prolapse	13

Table 2

Valve state predictor accuracy across all potential reference frames. *Closed valves* and *open valves* are those frames manually selected to contain a closed or open mitral valve, respectively. %Closed and %open indicate the percentage of frames in a category that the valve state predictor labeled as containing either a closed or open valve, respectively.

Data set	Closed valves		Open valves	
	%Closed	%Open	%Open	%Closed
1	100	0	100	0
2	100	0	100	0
3	100	0	100	0
4	93.1	6.9	100	0
5	100	0	100	0
6	100	0	100	0
7	100	0	100	0
Group	99.2	0.8	100	0

Table 3

RMS of the Euclidean distance of the automatically tracked annulus from the mean of the manually tracked annulus points.

Data set	RMS distance (mm) (mean ± std. dev.)	No. of open frames
1	1.96 ± 0.70	3
2	0.75 ± 0.06	4
3	2.30 ± 0.40	5
4	1.04 ± 0.07	5
5	1.71 ± 0.26	4
6	2.02 ± 0.38	6
7	1.86 ± 0.44	3
Group	1.67 ± 0.63	30

Table 4

RMS of the Euclidean distance of each experts' manually tracked annulus from the mean computed from the other two experts' manual segmentations and the CLKOF tracked annulus.

Data set	RMS distance (mm) (mean ± standard deviation)			No. of open frames
	Expert 1	**Expert 2**	**Expert 3**	
1	2.04 ± 0.30	3.02 ± 0.07	2.40 ± 0.51	3
2	0.83 ± 0.13	1.81 ± 0.08	1.16 ± 0.05	4
3	2.05 ± 0.19	3.01 ± 0.22	5.62 ± 0.86	5
4	0.66 ± 0.06	1.20 ± 0.17	1.14 ± 0.06	5
5	1.02 ± 0.21	1.98 ± 0.08	1.69 ± 0.34	4
6	1.83 ± 0.41	2.60 ± 0.36	1.50 ± 0.24	6
7	1.49 ± 0.33	3.01 ± 0.62	1.69 ± 0.05	3
Group	1.99 ± 1.15			30

Table 5

Distance between an annulus delineated using the CLKOF tracking method from an annulus segmented using the 3DMAS method for closed frames $n-1$ and $n+1$ neighboring the randomly selected frame n.

Data set	RMS distance (mm)	
	Frame$_{n-1}$	Frame$_{n+1}$
1	0.38	0.45
2	0.31	0.48
3	0.55	0.68
4	0.34	0.50
5	0.78	0.59
6	0.38	0.56
7	0.48	1.56
Avg. ± std. dev.	0.58 ± 0.31	